Polymer 50 (2009) 4018–4027

Contents lists available at ScienceDirect

Polymer

journal homepage: www.elsevier.com/locate/polymer

Characterisation and modelling of polypropylene/carbon nanofibre nanocomposites

Richard J. Foster, Peter J. Hine, Ian M. Ward*

Polymer and Complex Fluids Group, School of Physics and Astronomy, University of Leeds, Leeds, LS2 9JT, UK

ARTICLE INFO

Article history:
Received 9 May 2009
Received in revised form
15 June 2009
Accepted 16 June 2009
Available online 21 June 2009

Keywords:
Polymer composites
Carbon nanofibres
Nanocomposite

ABSTRACT

In this paper we describe the production of a polypropylene (PP)/carbon nanofibre (CNF) nanocomposite, and subsequent characterisation of the structure and properties of the nanocomposite material at various stages of blending. Dispersion of the CNF throughout the matrix PP was monitored by scanning electron microscopy (SEM), and analysis of the lengths of the individual CNF was estimated using dynamic light scattering (DLS). This latter technique enabled a comparison to be made between the measured Young's modulus of the material and that predicted by micromechanical modelling, using the fibre length as determined by DLS. The temperature performance of the nanocomposite material was determined, and this behaviour has also been modelled.

1. Introduction

Polymer nanocomposites have recently become the subject of intensive research. Although a wide range of properties, including toughness, creep and thermal stability have been investigated, improvement in the tensile mechanical properties of the composite are always an important consideration, and a number of different nanofillers have been reported in the literature.

Nanoclays, usually montmorillonite, are the most widely reported nanofiller (for a review see [1]) in the literature, although carbon nanotubes (CNTs) including both single (SWNT) and multi-walled (MWNT) varieties and cheaper vapour-grown carbon nanofibres (CNF) have all also been widely reported. The large majority of these studies have used polypropylene as the polymer of choice for reinforcement, and a number of the studies have shown improvement in the mechanical properties of PP (e.g. [2]).

Vapour-grown carbon nanofibres (CNF) are a cheaper alternative to MWNT and SWNT, and are available on a commercial scale. These CNF have been used in a number of different studies (e.g. Refs. [2–7]). Of particular note is the work of Kuriger and co-workers who have investigated a number of the processing parameters in blending CNF into polypropylene (PP) [8–10].

A key issue with nanofibre composites is how to blend the particles into the matrix in order to achieve good dispersion, whilst retaining a high nanofibre aspect ratio. A number of different blending strategies for CNF into PP have been suggested in the literature, including high shear mixing [3,9,10], ball milling the fibre assembly [3] and solvent dispersion [9,11], and although many have reported the changes in the mechanical properties, few authors have attempted to characterise the change in properties due to the CNF fibre length, and have instead focused on the problems of dispersion of the CNF throughout the polymer matrix. Exceptions to this are the work of Kuriger et al. [9] and Hine et al. [7], who used SEM micrographs to estimate the average CNF length post-blending, and subsequently used this length to estimate the reinforcement efficiency of the CNF.

Recently, it has been reported that dynamic light scattering (DLS) can be used to determine the length of SWNT and MWNTs [12,13]. This technique offers an alternative method of measuring the nanofibre length, with the advantage that light scattering samples over many fibres. This provides a better estimate of the average length, rather than the few hundred fibres that can be randomly sampled using image analysis in a reasonable time scale. However the model used, developed by Badaire et al. [12], to analyse the DLS does not possess sufficient sensitivity to determine CNF diameter.

The present study thus combined various elements from electron microscopy analysis with the DLS approach to estimate the average aspect ratio of the CNF after various blending strategies. The Cox–Krenchel micromechanical model [14] is then used to obtain an estimate of the nanocomposite tensile Young's modulus

* Corresponding author. Tel.: +44 0 113 3433808; fax: +44 0 113 3433846.
E-mail addresses: r.j.foster@leeds.ac.uk (R.J. Foster), p.j.hine@leeds.ac.uk (P.J. Hine), i.m.ward@leeds.ac.uk (I.M. Ward).

0032-3861/$ – see front matter © 2009 Elsevier Ltd. All rights reserved.
doi:10.1016/j.polymer.2009.06.033

and compared to the experimentally determined modulus. Electron microscopy has been used to ascertain the degree of CNF dispersion throughout the PP matrix.

2. Experimental

2.1. Materials

The polypropylene (PP) used in this work was a homopolymer with a weight average molecular weight (M_W) of 360,000 g/mol, number average molecular weight (M_n) of 78,100 g/mol, density of 910 kg m^{-3}, and a peak melting point of 163 °C.

Vapour-grown carbon nanofibres (CNF) were obtained from Pyrograf Products Inc, a division of Applied Sciences Inc, Cedarville, OH, and are designated as Pyrograf III™ PR-19-PS-LD. These are pyrolytically stripped fibres, where the polyaromatic hydrocarbons are removed from the surface of the fibres [15]. These CNF were obtained in a powder-like "soot" form, where the individual fibres are extremely entangled, as shown in Fig. 1. This highly entangled nature of the CNF results in a nanoscale filler that is difficult to disperse throughout the PP matrix, since the entangled assemblies must be broken up in order to achieve even dispersion throughout the composite, with an associated reduction in length.

2.2. Processing

As with a previous study by the authors [7], blending of CNF with PP was achieved using a twin-screw extruder, both for simplicity of processing and for potential commercial scalability. The high shear generated in the extruder barrel has been shown to sufficiently break apart the CNF aggregates [7–9].

The extruder used in this study was a Thermo Electron Corporation co-rotating twin-screw extruder, with length-to-diameter ratio of 40. A loading of 10%w/w (5%V/V) CNF was used. Blending temperatures of both 200 and 230 °C, and a screw speed of ~70 rpm, were used to produce the nanocomposite material, based on previous work by the authors [7], and that of Kuriger [8,9], as a guide to processing conditions.

Mixing schedules for the composite material are shown in Table 1. The extruder was set-up such that there were three individual mixing zones along the extruder barrel and all the CNF powder was introduced into the extruder before the final mixing zone in the first extrusion (which was not possible in previous work [7]). Multiple mixings of the composite were achieved by extruding the nanocomposite material several times, as indicated in Table 1.

The extruded PP/CNF nanocomposite material was then pelletised and pressed into compression moulded sheets in a hot press at 210 °C, nominally at a pressure of 0.07 MPa (100 psi) for three minutes before being increased to a final pressure of 1.2 MPa. The samples were held under this final pressure whilst being rapidly cooled in the platens of the press using circulated water.

Table 1
Mixing schedules for nanocomposite.

Blending temperatures (°C)	Number of extrusions	Number of mixing zones
200 and 230	1	1
	2	4
	3	7

2.3. Mechanical testing

Young's modulus of the nanocomposite material from the various mixing schedules was determined by static tensile testing on an RDP-Howden servo mechanical tensile testing machine. Dumbbell shaped samples were cut from the nanocomposite sheets, consistent with ASTM D638. Samples were tested at 21 °C, 50%RH, and a nominal strain rate of 5×10^{-3} s^{-1}.

Sample strain in the tensile tests was determined using a Messphysik video extensometer programmed to track targets painted onto the sample surface. To avoid sample straightening affecting the measurement of Young's modulus, a pre-load of approximately 1.5 MPa was applied before the start of each test.

2.4. Analytical techniques

A number of techniques have been reported to determine the effectiveness of the reinforcement provided by the CNF.

Techniques such in-situ optical image analysis on glass fibres [16] cannot be used with nanocomposite materials, since the fibres/particles are often too small to be seen with optical microscopes. Many researchers have used scanning electron microscopy (SEM) to image nanofibres and particles (e.g. Refs. [2,3,17–19]), however this means only a small number of nanofibres can be imaged in a reasonable timescale, and leads to poor statistics.

Two different analytical techniques were used to study the produced nanocomposite:

1. Removal of CNF from the blended PP/CNF pellets by ashing of the composite and subsequent observation of the residue using SEM. Fibre diameter was measured from this residue.
2. Removal of CNF from the blended PP/CNF pellets by chemical dissolution of the PP and subsequent hot filtration technique. Dynamic light scattering (DLS) was used to determine the average fibre length of the removed CNF.

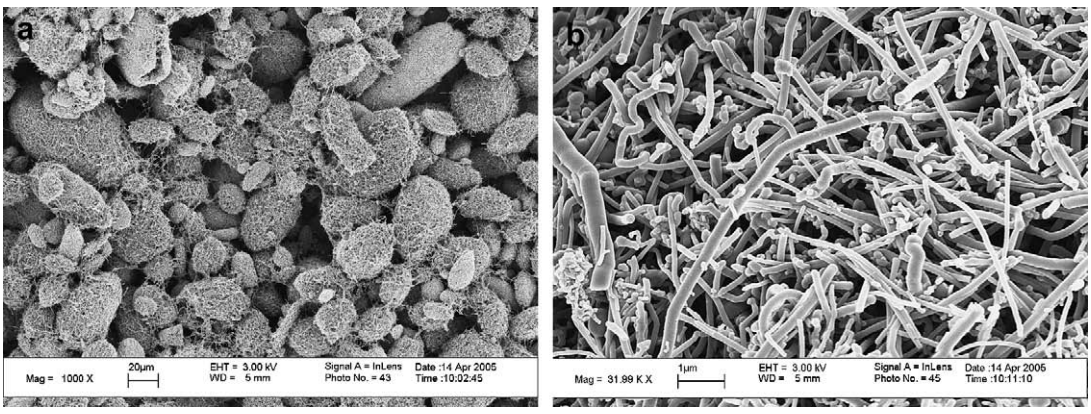

Fig. 1. Scanning electron micrographs of CNF bundles (a). Low magnification (b). High magnification of one of the bundles.

2.4.1. Ashing of composite

PP/CNF pellets (~2 g) from each stage of blending at each blending temperature were heated in a crucible at 400 °C for 2.5 h, in order to completely vaporize the PP, leaving only the CNF. The CNF residue from the ashing process was then separated, dispersed in a deionised water/surfactant (sodium dodecyl sulphate) and stirred. A small amount was then placed onto an SEM stub for observation. Previously, this technique was used successfully for both qualitative and quantitative (measurement of fibre length and diameter) analysis of CNF composites [7].

2.4.2. Scanning electron microscopy (SEM)

Qualitative analysis of the as-received CNF, the residue of the ashed composite and the fibres in-situ within the nanocomposite was achieved using SEM imaging. All samples were sputter-coated with platinum (thickness of 3 nm) in an argon plasma before observation in a LEO1530 FEGSEM.

The as-received CNF were placed directly onto an SEM stub (both with and without a carbon base pad). The residue of the ashed composite was removed from the crucible and placed directly onto an SEM stub with a conducting carbon base pad.

Residue of material was observed from all three mixing schedules (1, 4 and 7 mixing zones) and both blending temperatures. Imaging of the PP/CNF nanocomposite material in-situ involved observing 'freeze fractures' of produced compression moulded sheets. Small pieces of the compression moulded sheets were immersed in liquid nitrogen for ~30 s before being fractured. The fracture surfaces were then observed after mounting on the SEM stub with carbon base pad. Observations were made of the compression moulded sheets produced from each batch of blended material (i.e. both blending temperatures and all mixing schedules). Silver paint was coated down one edge to improve sample conductivity.

2.4.3. Image analysis of SEM images to determine CNF diameter

A number of SEM images of the as-received CNF residue from ashed composite and CNF in-situ in the nanocomposite were analysed to measure the CNF diameter, d_f. A simple image analysis tool was used to obtain the average diameter of 220 nanofibres. The measurements were calibrated to the scale bar present on all images obtained from the SEM. Measurements of d_f were made in this fashion since fitting of dynamic light scattering (DLS) autocorrelation functions using a model by Badaire et al. [12] was shown to be highly insensitive to the value of d_f chosen.

2.5. Dynamic light scattering (DLS)

SEM analysis showed the tendency of the CNF to re-aggregate into large agglomerates, and so it was not possible to determine CNF length using this technique. Instead CNF were removed from the pellets by dissolving 2 g of PP/CNF pellets in 200 ml of xylene in a 2 l round bottomed flask. A condenser was placed on the top of the flask to prevent escape of vapour. The xylene–PP/CNF mix was brought to the boil (~140 °C) and refluxed for a minimum 20 min. The mixture was then visually inspected to ensure that all the PP/CNF pellets had dissolved and that no aggregates of CNF had formed.

The xylene and dissolved PP and CNF were then filtered through a sintered glass filter (porosity grade 5, pore size 4–10 μm), heated to 140 °C in order to prevent the PP in the mixture cooling and solidifying within the filter, clogging it up. During filtration, negative pressure was applied across the filter, and the sinter was periodically washed with hot xylene to prevent any PP solidifying within the glass sinter. Following filtration, the sintered glass filter was backwashed with a deionised water/sodium dodecyl sulphate (SDS), a surfactant, solution (1%w/w SDS), periodically gently scraping the surface of the filter to dislodge CNF from the sinter surface, into the deionised water/SDS solution. The final CNF/deionised water/SDS solution was estimated at a concentration of ~0.1%w/w CNF.

For the dynamic light scattering measurements, CNF/deionised water/SDS solutions were produced from the PP/CNF pellets manufactured at each stage of mixing (1, 4 and 7 mixing zones). The dilute solutions (~0.1%w/w CNF) were then diluted further with deionised water/SDS solution, such that the CNF solution was $<10^{-3}$%w/w CNF. This followed the method set out by Badaire et al. [12], and was suggested to be an optimal fraction of CNF such that aggregation was avoided, yet a strong scattering signal was generated from the sample.

The DLS set-up comprised of a Spectra-Physics 2016 Ar+ laser, and an ALV DLS/SLS-5000 compact goniometer system. Samples were contained within a cylindrical cuvette, which was placed in a toluene bath. The bath was temperature controlled at (298 ± 0.2) K. 100 mW coherent light of 488 nm was used to illuminate the sample, and spectra were correlated at 30°. All runs were performed with the polarisers in the vertical position (maximum intensity). Runs were performed and the scattering was measured from the sample for an hour.

Autocorrelation functions obtained from the DLS runs were then fitted with the model for rod-like particles developed by Badaire et al. (Ref. [12]). CNF diameter (d_f), was fixed to that determined by SEM image analysis, because, as discussed, the model was insensitive to the value of d_f chosen.

3. Results

3.1. Young's modulus

The variation in tensile Young's modulus of PP/CNF nanocomposite versus number of mixes is shown in Fig. 2 for material blended at both 200 (squares) and 230 °C (triangles). The optimum (peak) tensile Young's modulus in the compression moulded sheet blended at 200 °C was for material that had been mixed through 4 mixing zones. The peak in Young's modulus of nanocomposite material blended at 230 °C is much less distinct, because the viscosity of the polymer decreases with increasing temperature. This means that the shear forces exhibited on the CNF 'bundles'

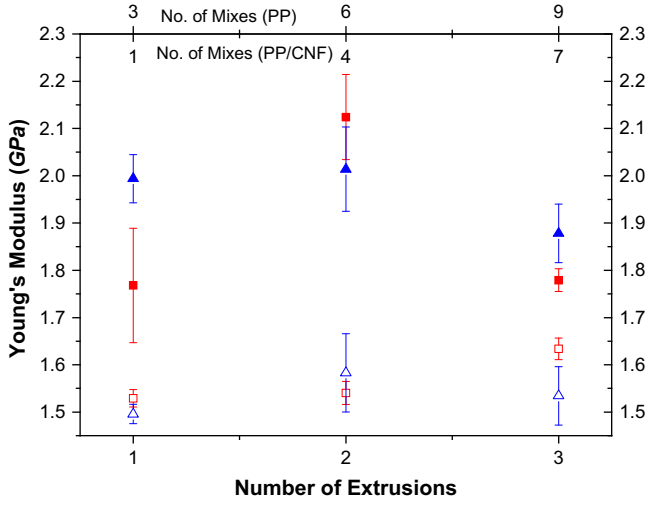

Fig. 2. Tensile Young's modulus of compression moulded sheets of PP/CNF nanocomposite material blended at 200 (■) and 230 °C (▲). As a comparison, the tensile modulus of pure PP material blended in the same mixing schedules as the nanocomposite is shown, blended at both 200 (□) and 230 °C (△).

decrease with increasing temperature, and so a sharp peak in Young's modulus is not seen.

For the material blended at 200 °C, Young's modulus of the material was seen to increased from (1.8 ± 0.1) GPa at one mix, to (2.12 ± 0.09) GPa for material mixed four times and finally decreased to (1.78 ± 0.02) GPa for material mixed seven times. The peak Young's modulus in the PP/CNF material blended at 200 °C is similar to that measured by Hine et al. [7], who used a similar mixing schedule at a loading of 10%w/w CNF.

A further point to consider is that the true peak in Young's modulus may not be seen for the 230 °C blended nanocomposite material. Since the properties of the nanocomposite material were only determined for material that has been mixed through one, four and seven mixing zones (one mix on the first extrusion and then three on each subsequent extrusion), it is possible that the peak Young's modulus for the material at this blending temperature may be at some other number of mixes.

The variation in Young's modulus of the nanocomposite twin-screw extruded nanocomposite material mirrors that seen in the work of Kuriger [10], who showed that an increase in Young's modulus was observed by an increase in blending temperature. The difference in the present work, where the lower blending temperature shows a higher Young's modulus, could be due to the different viscosity of the polypropylene used in this study, compared to that of Kuriger [10].

It is suggested that the change in tensile Young's modulus with increasing amount of mixing is due to two competing factors, that of improved dispersion of CNF throughout the PP, and reduction in CNF length with an increased amount of mixing. The analysis performed on the nanocomposite material (discussed below) supports this hypothesis.

In addition, Fig. 2 shows the results of tensile tests performed on compression moulded sheets of pure PP, having been through the same blending process in the twin-screw extruder as the nanocomposite material. The pure PP material shows no variation with the amount of mixing, and no variation with blending temperature. The average value for the pure PP material was determined to be (1.55 ± 0.01) GPa. This indicates that there was no degradation of the polymer with the amount of mixing, and also that the variation in Young's modulus with mixing is entirely due to the incorporation of the CNF into the PP.

Although previous authors have suggested that the inclusion of a compatibiliser, such as maleic anhydride grafted polypropylene, can further improve the tensile properties of a nanocomposite [20], previous work has shown that with CNF (and using the same blending strategy), there is no significant improvement in Young's modulus [21].

3.2. Scanning electron microscopy (SEM)

3.2.1. Ashed composite residue

Residues of the ashed composite were observed under SEM from pellets of the PP/CNF nanocomposite blended at both 200 and 230 °C, and from one, four and seven mixing zones. These were compared to the as-received CNF, as shown in Fig. 1 The images clearly show the highly entangled nature of the CNF when received, and also the 'bundles' formed by the CNF, which range in size from approximately 500 nm to 30 μm. From these images, it becomes evident that even if the manufacturer's estimated length of 10–100 μm [15] is found in the as-received CNF, these longer fibres must be highly entangled and cannot possibly be straight. This suggests that any attrition of the CNF bundles must break fibres, and result in shorter fibre lengths than production estimates.

The fibre residue of the nanocomposite material passed through one mixing zone (a single extrusion), blended at 200 °C, is shown in Fig. 3(a). It can be seen that several of the CNF bundles are still visible, a considerable number of which are similar in size to the CNF bundles seen in the as-received fibres, suggesting that the amount of mixing subjected to the CNF bundles during a single extrusion is insufficient to break apart the CNF bundles and disperse the fibres throughout the PP matrix. The bundles, however, do look as though they have been broken up to a certain extent, as there are a number of the bundles that are more diffuse than the highly entangled states seen in Fig. 1.

SEM images of the residues of ashed composite material mixed four and seven times show a completely different CNF bundle structure to that seen for the composite material mixed once, as seen in Fig. 3(b). These images show that the residue fibres have formed highly entangled 'mats' of material, rather than retaining the ball-like structures seen in the as-received fibres, and have formed because of the tendency of the CNF to aggregate due to their high surface energy. The mats of CNF are believed to form during the ashing process, since as the polypropylene vaporizes in the oven, a bubble of PP is formed, forcing all the CNF to surface of this bubble, where they re-aggregate into the mats observed in Fig. 3(b).

Although this re-aggregation does mean that it is extremely difficult to obtain any direct measurements of the CNF aspect ratio (the high degree of fibre entanglement means that it is extremely difficult to determine fibre length), it can be inferred from these images that the CNF must be well dispersed within the PP matrix. If this were not the case, the bundles of CNF as seen in the residue of the ashed composite that had only been mixed once, would also be observed in these images, and the CNF mats would not have formed in such a distinct fashion.

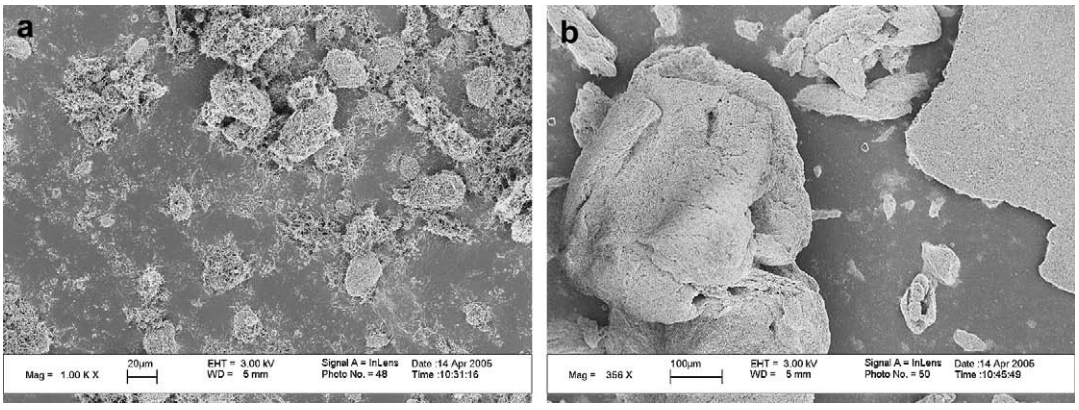

Fig. 3. Fibre residue of ashed PP/CNF nanocomposite material blended at 200 °C. (a) A single mixing zone (one extrusion). (b) Seven mixing zones (three extrusions).

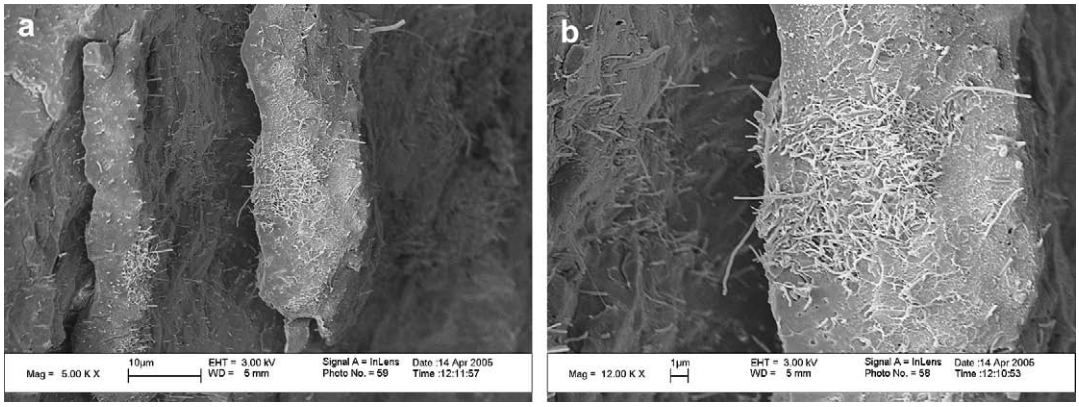

Fig. 4. SEM image of freeze-fractured nanocomposite material blended at 200 °C, and passed through a single mixing zone (one extrusion). (a) Low magnification image showing large clumps of CNF bundles in the composite material. (b) Higher magnification image of a clump of CNF fibres in-situ in the composite material. Also visible are a number of voids in the regions of high fibre density. The size of the bundle seen at A is similar in size to the as-received bundles seen in Fig. 1.

3.2.2. *Freeze-fractured composite*

Freeze-fractures of the nanocomposite material processed through a single mixing zone, and blended at 200 °C, are shown in Fig. 4. Clearly visible in these two images are large clumps of CNF in the nanocomposite and regions of unwetted fibres, a positive indication that the CNF bundles have not been broken up and the fibres dispersed evenly throughout the PP matrix as seen in the extracted fibres. Also visible, particularly in the higher magnification image, are the presence of voids in the material, signifying that not all the fibres in the material had been wetted by the matrix material during the blending process. Further to this, there are large regions of pure PP matrix material with no fibres present. Similar aggregations, although not on such a widespread scale, were also seen in the material blended at 230 °C.

These images clearly suggest that a single mixing zone is insufficient to break apart the CNF bundles in the as-received fibres and to evenly disperse the fibres throughout the PP matrix. This explains the low measured Young's modulus of the nanocomposite material, as shown in Fig. 2.

SEM images of the freeze-fractures of the PP/CNF nanocomposite material blended through four and seven mixing zones are shown in Fig. 5. These images show an even dispersion of the nanofibres throughout the PP matrix which suggests that four mixes is sufficient in order to break up the bundles seen in the as-received fibres, and disperse the fibres throughout the matrix. This confirms the hypothesis that the improvement in Young's modulus shown in Fig. 2, seen in the material mixed four times over that mixed once, is due to an improved dispersion. From these SEM images, however, it was difficult to ascertain if there was any change in the length of the fibres in increasing the amount of mixing from four to seven mixing zones, because it the fibres were often continued in the bulk material and were thus buried.

3.3. *Measurement of fibre aspect ratio*

A key aspect of this study was to use modelling to link the structure of the PP/CNF nanocomposite to the experimentally determined properties, and so understand the loss in properties as the amount of mixing was increased from four to seven mixing zones. The most important aspect of the modelling is the determination of the fibre aspect ratio at each stage of blending. This was done through a combination of scanning electron microscopy (SEM) image analysis to determine the CNF diameter and dynamic light scattering (DLS) in order to measure the CNF length.

3.3.1. *Measurement of fibre diameter by image analysis*

The CNF fibre diameter was determined by measuring 220 fibres from SEM images, including fibres from pre and post blended CNF. The mean fibre diameter, determined as the mean of all 220 average CNF diameters, was found to be (93 ± 3) nm. The distribution of fibre diameters, binned into blocks of 10 nm, is shown in the histogram in Fig. 6.

This measured fibre diameter is slightly smaller than the 100–200 nm diameter range estimated by the CNF manufacturer, Applied Sciences Inc [15], and the diameter estimated by Patton et al. [22] and Tibbetts and co-workers [3,6]. It is however, similar to the measurement of CNF diameter determined by Hine et al. [7] and as estimated by Brandl et al. [23].

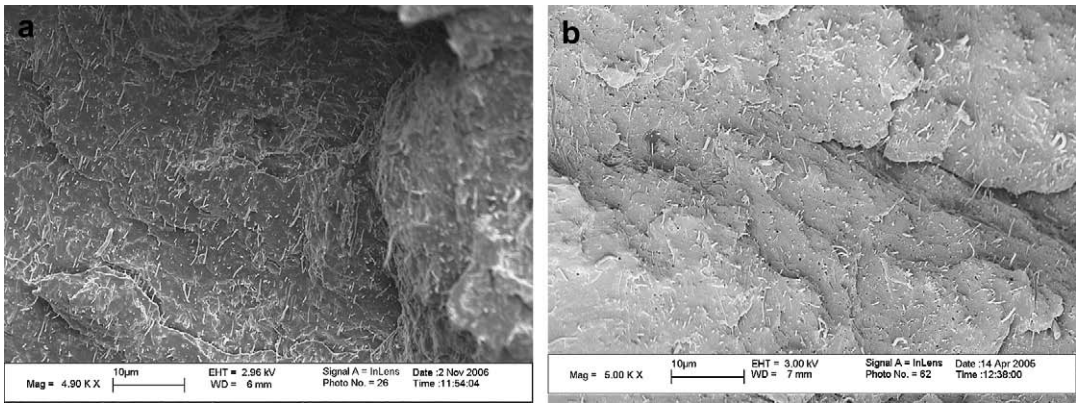

Fig. 5. SEM image of freeze-fracture of nanocomposite material blended at 200 °C. (a) mixed four times (two extrusions), (b) Mixed seven times (three extrusions).

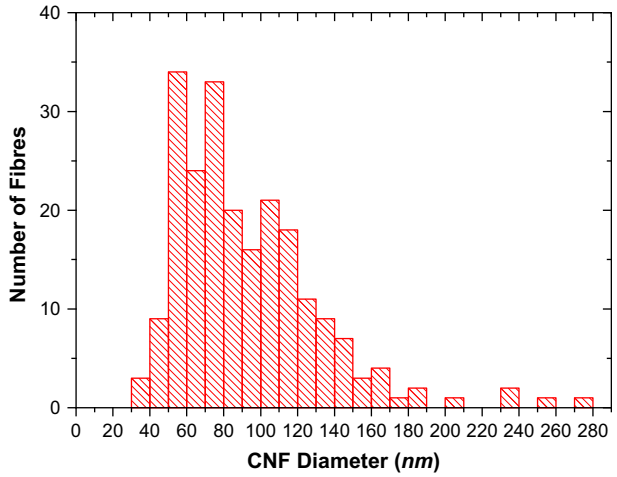

Fig. 6. Histogram of CNF diameters determined by SEM image analysis. The data was binned into 10 nm steps. A total of 220 fibre diameters were determined and the number average diameter was determined to be (93 ± 3) nm.

3.3.2. *Measurement of fibre length by dynamic light scattering*

A number of other studies [3,6,7] have used SEM image analysis to determine a measurement of the post-blending CNF length, however these determinations only measured a few fibres in order to determine fibre length (e.g. Hine et al. [7] only measured a total of ~100 fibres, resulting in a large error in l_f). Compared to the number of CNF in a typical dumbbell tensile testing specimen, of the order of 10^6 fibres, SEM can obviously only determine the length of a fraction of the fibres in such sample.

Measurement of fibre length is not only critical in being able to model the properties of the composite, it also varies from fibre to fibre in the sample, depending on where the original CNF fractures during the blending process. A number of studies have shown defects and anisotropy in both CNF and nanotubes, and have shown that these are more likely to act as weak-points for fracture. This makes the length of the CNF highly variable and so it is desirable to measure a large number of the fibre lengths in order to obtain an accurate determination of the length, especially if the changes in length due to an increased amount of mixing are small.

Previous SEM image analysis, and that performed in this study, has shown that this technique is extremely difficult to expand to cover a wide range of fibres. The measurement of the diameter of the CNF in this study required 220 fibres in order to obtain a good average of the diameter, and to determine the distribution of fibre diameters. Considering that the CNF diameter is unaffected by the high shear mixing process, an image analysis study of enough CNF lengths would be prohibitively time consuming. In addition to this, the CNF residues tended to re-aggregate into large agglomerated 'mats' of CNF, meaning that it was difficult to get more than a hundred isolated fibres where the length could seen clearly. The images of the CNF embedded in the composite could not be used, as it is difficult to determine whether the entire fibre is visible is such an image.

Samples of the PP/CNF nanocomposite blended at 200 °C and passed through four and seven mixings zones were analysed. Unfortunately, the CNF sample blended through a single extrusion (one mixing zone) still had large aggregations in the solution (since the blending process had not broken up the CNF bundles completely), and so good scattering could not be obtained from these samples.

The model developed by Badaire et al. [12] uses a number of parameters to fit the autocorrelation scattering function obtained from the DLS. These parameters are the fibre length, l_f, fibre diameter, d_f, scattering wavevector, (dependent on scattering angle, laser wavelength and refractive index of the solution) and a parameter, α, that is analogous to the polydispersity, describing the breadth of the distribution of fitted fibre aspect ratio. Trial fitting of this function on the autocorrelation scattering functions from the DLS showed that the fitting was highly insensitive to the fibre diameter, so this was fixed at 93 nm, from the SEM image analysis. The wavevector was calculated from the scattering angle, refractive index of the solution and laser wavelength.

The autocorrelation functions and fits of the model to the autocorrelation functions are shown in Fig. 7. The fitted parameters to the autocorrelation functions are shown in Table 2. As the amount of mixing on the nanocomposite was increased, the fitted length of CNF decreased from 3.175 μm to 2.66 μm. This corresponded to a reduction in the fibre aspect ratio from (34 ± 1) to (28.7 ± 0.8). In addition to this, the 'polydispersity' of the fit increased from 0.67 to 0.925, suggesting that the distribution of lengths became narrower with increased mixing.

The Badaire model fit to the DLS autocorrelation function from the CNF hot filtrated from the nanocomposite blended at 200 °C through seven mixing zones was not fitted to the entire dataset, because it was found that if a fit over the entire range was attempted, the model did not fit the data in the 'knee' region of the autocorrelation function because of the large fluctuations in data at longer correlation times.

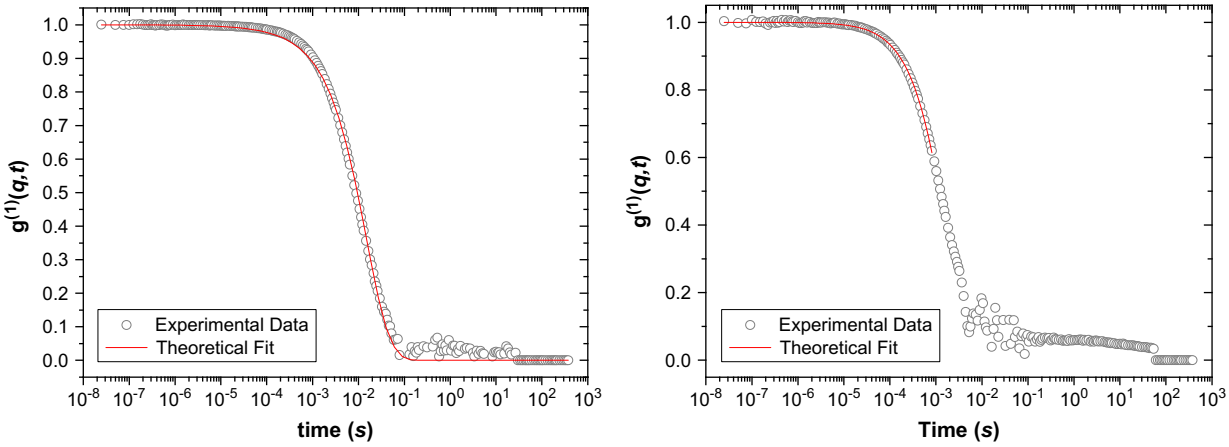

Fig. 7. Autocorrelation scattering functions from DLS for nanocomposite material. Left pane shows CNF blended at 200 °C through 4 mixing zones. The Badaire model from Ref. [12] gave a fitted CNF length of 3.18 μm, and polydispersity of 0.67. The right pane shows CNF blended at 200 °C through 7 mixing zones. The Badaire model from Ref. [12] gave a fitted CNF length of 2.66 μm, and polydispersity of 0.93.

Table 2
Fitted parameters of the DLS autocorrelation scattering functions, using the model developed by Badaire et al. [12]. The fibre aspect ratio was determined by l_f/d_f.

Number of mixing zones	Fitted fibre length, l_f (μm)	Fitted 'polydispersity,' α	Fibre aspect ratio
4	3.18	0.67	34 ± 1
7	2.66	0.93	28.7 ± 0.8

Investigation of Badaire model [12] showed that the short time part of the autocorrelation function was the most significant in determining the length of the CNF. The long timescale scattering does not affect the length obtained, and can be ignored when fitting the data.

An important consideration concerning the values obtained for the CNF after 4 and 7 mixing zones is that the Badaire et al. [12] model was developed for rigid rod-like multi-walled nanotubes, where it is a reasonable assumption that the CNTs are straight. From the SEM images shown in this study, this is not the case for CNF. The DLS data therefore represents a CNF length if the fibres were straight, and so is likely to be an underestimate of the true CNF length. As a check, image analysis of a small number of CNF from a single SEM image of extracted fibres gave a CNF length in the range of 2–3 μm, similar to that determined by DLS.

4. Micromechanical modelling

4.1. Cox–Krenchel model

The Cox–Krenchel model [14], as given by Equation (1), was used to predict the properties of the nanocomposite material, using the Cox (η_l) [24] and Krenchel [25] efficiency factors (η_o) to account for fibre length and fibre orientation respectively:

$$E_C = \eta_o \eta_l E_f V_f + E_m V_m \tag{1}$$

The Cox efficiency factor is given by [14]:

$$\eta_l = \left(1 - \frac{\tanh \beta l_f/2}{\beta l_f/2}\right) \tag{2}$$

where l_f is the length of the fibre and β is given by [14]:

$$\beta = \left(\frac{2G_m}{E_f r_f^2 \ln\left[\left(2\sqrt{3}V_f/\pi\right)^{\frac{1}{2}}\right]}\right)^{\frac{1}{2}} \tag{3}$$

where G_m is the shear modulus of the matrix, E_f is the fibre modulus, r_f is the fibre radius and V_f is the fibre volume fraction. The Krenchel efficiency factor is given by [14]:

$$\eta_o = \int a_n \left\langle \cos^4 \theta_n \right\rangle d\theta \tag{4}$$

where θ_n is the angle between fibre axis and loading axis, and a_n is the proportion of fibres at this angle. Both random in-plane (2D) and random 3D fibre orientations were considered in this study, thus η_o was taken be $^3/_8$ (2D) or $^1/_5$ (3D).

The material properties used in this work are detailed in Table 3, and are a mixture of experimentally determined values and estimated values from the literature. The Cox–Krenchel model was used to calculate the PP/CNF modulus, using the axial Young's modulus determined by Tibbetts [26].

Table 3
Fibre and matrix material properties used in modelling.

Carbon nanofibre properties	E_{11}	240 GPa	Literature [26]
Polypropylene	E	(1.55 ± 0.01) GPa	Measured
	ν	0.35	Literature/measured [7]

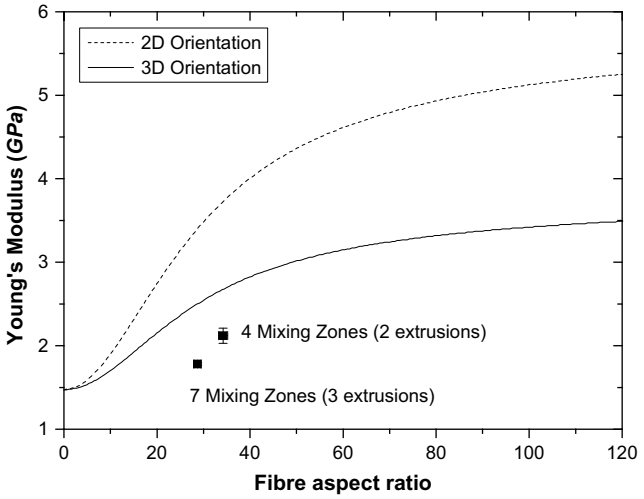

Fig. 8. Prediction of PP/CNF nanocomposite Young's modulus versus the fibre aspect ratio for fibres oriented randomly (3D) and randomly in-plane (2D) CNF fibres. Also shown are the experimentally determined Young's modulus versus aspect ratio for the compression moulded sheets produced from the nanocomposite mixed 4 and 7 times. The error bars are the standard error in each measurement.

4.1.1. Comparison of Cox–Krenchel predictions to experimentally measured Young's modulus

The variation of the nanocomposite Young's modulus with fibre aspect ratio, as predicted by the Cox–Krenchel model, is shown in Fig. 8. A comparison between the experimentally determined Young's modulus of the compression moulded nanocomposite PP/CNF sheets produced from the blended material that passed through four and seven mixing zones is also shown. The aspect ratios for the reinforcing fibres were determined as described above (Section 3.3). The modelled Young's modulus at the same aspect ratio as measured for the fibres from the nanocomposite material mixed 4 and 7 times, is shown in comparison to the experimentally determined modulus in Table 4.

Although Young's modulus predicted by the Cox–Krenchel model is of the same order of magnitude as the experimentally determined Young's modulus; the model does significantly overestimate the modulus in comparison to the experimentally determined value. There are a number of possible reasons for this, two of which have been investigated here: fibre dispersion is not perfect and so there is some clustering of fibres, and also that the value reported in the literature for the stiffness of the Pyrograf III™ CNF is an overestimate of the true value. These are discussed below.

Another possible (and highly probable) reason for the overestimate of Young's modulus of the nanocomposite material is that the Cox–Krenchel model assumes that all the fibres are straight, and thus stress transfer is uniform along the fibre length (except at the ends of the fibre [27]). As can be seen from the scanning

Table 4
Comparison of experimental determined Young's modulus and Cox–Krenchel predictions at the measured fibre aspect ratios.

Number of mixing zones	Fibre aspect ratio	Experimentally measured Young's modulus (GPa)	Cox–Krenchel Young's modulus prediction (GPa)	
			2D	3D
4	34 ± 1	2.12 ± 0.09	3.80 ± 0.04	2.71 ± 0.03
7	28.7 ± 0.8	1.78 ± 0.02	3.46 ± 0.05	2.53 ± 0.02

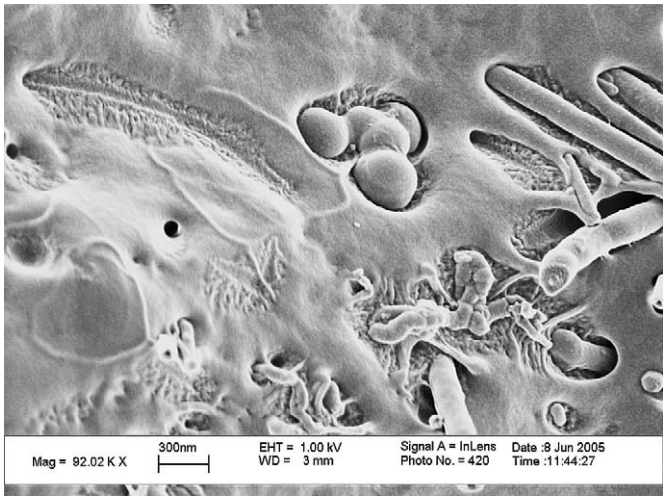

Fig. 9. High magnification SEM images of a freeze-fracture surface of the composite showing the CNF in-situ in the PP matrix, where the transcrystalline zone can be seen surrounding the CNF, and amorphous carbon is also seen in material.

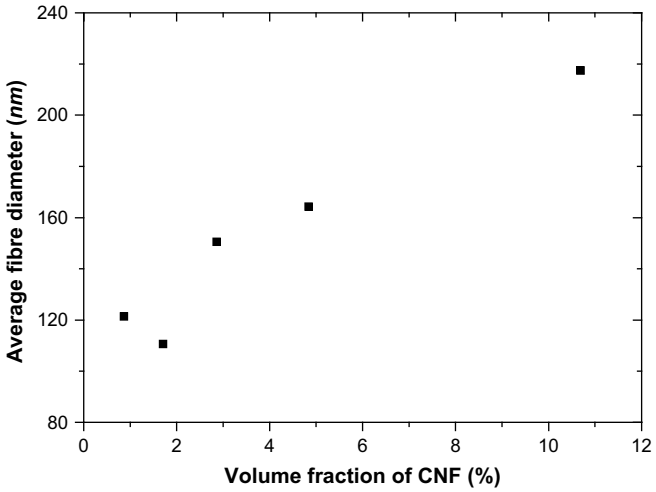

Fig. 10. Estimation of average fibre diameter versus volume fraction of CNF, calculated from the variation in Young's modulus with increasing volume fraction. Estimates were made using the aspect ratio of 34 determined in this study.

electron microscopy (SEM) images, both prior to and after blending, the fibres are not straight, and there are also lumps of amorphous carbon in the composite material. Both fibres that significantly deviated from a rod-like particle, and amorphous carbon pieces, will have a considerable impact on the measured nanocomposite modulus.

A further reason is the aforementioned presence of a large transcrystalline zone sheathing each of the CNF, as can be seen in Fig. 9. This material has been seen surrounding all the CNF in the matrix and since it is composed of row crystallised polymer molecules nucleating on the CNF surface, the matrix in the transcrystalline zone will have markedly different properties to the bulk matrix. Since the properties of the interface region in composites are extremely difficult to determine, it is unclear how this will affect the composite model.

4.1.2. Clustering of fibres

Any aggregation of fibres in the composite will reduce the effective surface area that can be wetted by the matrix polymer, and so the stress transfer from matrix to fibres is reduced, and consequently, the stiffness of the composite sheet is also reduced.

Instead of using the Cox–Krenchel model to predict the nanocomposite properties, the calculation using Equation (4) was reversed to numerically match the experimentally determined Young's modulus to the effective aspect ratio of CNF aggregate with increasing volume fraction of CNF. In order to do this, the greatest discrepancy between the model and experimentally determined Young's modulus was used, i.e. using the Cox–Krenchel model with $\eta_o = {}^3/_8$ (random in-plane fibre orientation).

The results of these predictions are shown in Fig. 10. These results suggest that even with the larger aspect ratio measured in this study, an average diameter only two and half times greater than that measured in the SEM image analysis would account for the discrepancy between the predicted modulus from the Cox–Krenchel model and the experimentally determined Young's modulus.

Fig. 11 shows the effect of this clustering, in comparison to the predicted Young's modulus. It can be seen that if an average of two fibres are clustered, since the aspect ratio is halved, the experimentally determined Young's modulus is much closer to following the predicted Young's modulus from the Cox–Krenchel model. The material mixed 4 times now falls between the predictions for random 2D and 3D fibre orientations, and the material mixed 7 times falls just below the prediction for a random 3D orientation. These results are summarised in Table 5.

Although unlikely to be the sole reason for the Cox–Krenchel model over-predicting the nanocomposite Young's modulus, fibre clustering does provide a realistic explanation for the discrepancy between the model and the experimentally determined Young's modulus, given the propensity of the CNF to aggregate.

The Cox–Krenchel model also makes a number of assumptions: that the fibres are all identical, straight, have the same stiffness and bonding between the fibre and matrix is perfect. Fig. 9 shows that in the PP/CNF composites produced in this study do not obey all these assumptions. Curved fibres are visible, surrounded by a clear transcrystalline zone, and amorphous carbon can also be seen in the composite.

5. Temperature dependence of Young's modulus

A significant advantage of incorporating CNF into PP is the improvement in stiffness of the nanocomposite at elevated temperatures. Hine et al. [7] showed that the incorporation of CNF

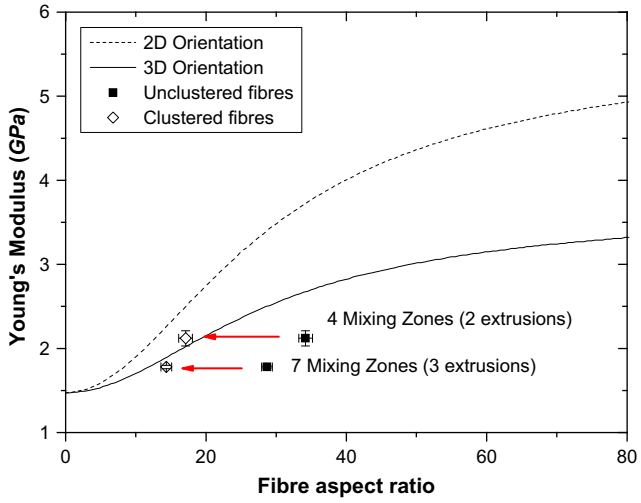

Fig. 11. Variation in predicted Young's modulus versus fibre aspect ratio, showing a comparison with the experimentally determined Young's modulus with aspect ratio assuming all fibres are separated in the matrix (■) and where, on average, two fibres are clustered (◇).

Table 5
Comparison between Cox–Krenchel predictions for clustered fibres (average of 2) and unclustered fibres.

Number of mixing zones	Experimentally measured Young's modulus (GPa)	Unclustered fibres (GPa)		Clustered fibres (3D), average of 2 fibres (GPa)
		2D	3D	
4	2.12 ± 0.09	3.80 ± 0.04	2.71 ± 0.03	2.04 ± 0.04
7	1.78 ± 0.02	3.46 ± 0.05	2.53 ± 0.02	1.90 ± 0.03

not only improved the stiffness of the nanocomposite up to 130 °C, but also that the percentage reinforcement effect was much greater than at room temperature.

The dynamic mechanical analysis (DMTA) performed on the nanocomposite material (a compression moulded sheet produced from the nanocomposite extruded twice/4 mixing zones was tested) is shown in Fig. 12. As with the results reported in Ref. [7], the stiffness of the nanocomposite is increased at all temperatures up to 140 °C and the percentage reinforcement effect was also increased.

The incorporation of CNF also has the added advantage of extending the 'useability window' of the composite, as for a specified modulus, the operating temperature window is extended (i.e. for a given modulus, e.g. 0.5 GPa, the incorporation of CNF extends the use of the composite from temperatures up to 80 °C, for the pure PP, to temperatures up to 120 °C for the nanocomposite).

5.1. Modelling of temperature performance using Cox–Krenchel model

The storage modulus of the PP/CNF nanocomposite, measured by DMTA, was also compared to the predicted modulus, using the Cox–Krenchel model.

Two different approaches have been made to this modelling; firstly using the aspect ratio measured for the nanocomposite (i.e. 34 ± 1, since the tested sheet was from the material mixed through four mixing zones). This approach obviously overestimated the PP/CNF modulus (as with the comparison with Young's modulus determined by static testing), so in order to investigate the effect of testing temperature on the PP/CNF material, a second approach was taken where a combined efficiency factor, η, was calculated from the room temperature moduli of the pure and composite material. This efficiency factor was then fixed over the whole temperature range, i.e. the only changing parameter was Young's modulus of the PP matrix, as measured by DMTA. These two modelling approaches are shown in comparison to the experimentally determined elastic moduli in Fig. 12.

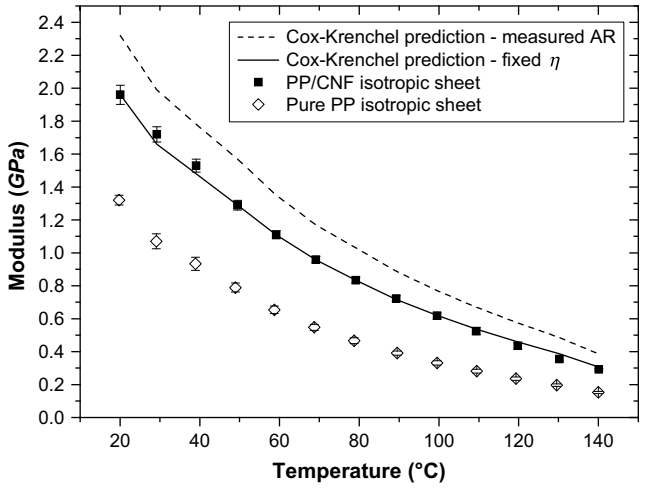

Fig. 12. Storage modulus of pure PP (◇) and PP/CNF nanocomposite (■), produced from the material mixed 4 times, versus testing temperature, measured by DMTA. A comparison of storage modulus predicted by the Cox–Krenchel model, using both the Cox and Krenchel efficiency factors determined previously and also by fixing a combined efficiency factor using the room temperature moduli of the PP/CNF and PP from the DMTA scans.

It can be seen that, as expected, the predictions of the Cox–Krenchel model using the aspect ratio measured above, overestimate the modulus of the nanocomposite material at all temperatures, as with the comparison to Young's modulus determined by static testing. It can be seen though, that the predicted decrease in modulus closely matches the behaviour seen in the elastic modulus of the PP/CNF DMTA scan. This is further confirmed when considering the model with the efficiency factor fixed by the room temperature moduli of the PP/CNF and PP (i.e. the model is constrained to fit these two points, and then is allowed to run over the temperature range measured). The predicted modulus closely matches the behaviour of the PP/CNF scan, using this method of modelling the nanocomposite.

This latter way of modelling the nanocomposite is useful since the only changing parameter in the Cox–Krenchel model, with increasing temperature is the change in Young's modulus of the PP matrix. The excellent agreement between the DMTA scan of the nanocomposite and the model therefore indicates, as expected, that the CNF modulus varies very little in the temperature range studied, and so the only change in the composite material is the softening of the matrix as the temperature is increased.

6. Conclusions

Analysis of the blending of carbon nanofibres (CNF) with polypropylene (PP) has shown that there is a blending strategy that optimises Young's modulus of the resultant composite material, which in this study was by passing the material through four mixing zones in the extruder at 200 °C. Scanning electron microscopy has showed that with fewer mixes, the CNF are poorly dispersed through the composite, and with increased mixing dynamic light scattering indicates a significant reduction in the CNF length.

Micromechanical model predictions, based on the measured fibre aspect ratio over-predict the measured Young's modulus. A number of possible factors that reduce the 'effective' fibre aspect ratio have been postulated, including clustering of fibres, curved fibres, spherical amorphous carbon, overestimation of the fibre modulus and an interface region between the fibre and matrix.

Acknowledgements

The authors wish to thank the University of Leeds Nanomanufacturing Institute for funding R. Foster for his PhD and for purchase of the twin-screw extruder used in this work. Also Dr. Tom Waigh for use of his DLS equipment, and Drs. M. Tassieri and A. Papagiannopoulos for their help and assistance.

References

[1] Fischer H. Materials Science & Engineering C 2003;C23:763.
[2] Kumar S, Doshi H, Srinivasarao M, Park JO, Schiraldi DA. Polymer 2002;43(5):1701–3.
[3] Tibbetts GG, McHugh JJ. Journal of Materials Research 1999;14(7):2871–80.
[4] Finegan IC, Tibbetts GG, Glasgow DG, Ting J-M, Lake ML. Journal of Materials Science 2003;38(16):3485–90.
[5] Lozano K, Barrera EV. Journal of Applied Polymer Science 2001;79(1):125–33.
[6] Van Hattum FWJ, Bernardo CA, Finegan JC, Tibbetts GG, Alig RL, Lake ML. Polymer Composites 1999;20(5):683.
[7] Hine PJ, Broome V, Ward IM. Polymer 2005;46(24):10936–44.
[8] Kuriger RJ, Alam MK, Anderson DP. Journal of Materials Research 2001; 16(1):226.

[9] Kuriger RJ, Alam MK, Anderson DP, Jacobsen RL. Composites – Part A: Applied Science and Manufacturing 2002;33A(1):53–62.
[10] Kuriger RJ, Khairul Alam M. Polymer Composites 2001;22(5):604–12.
[11] Kearns JC, Shambaugh RL. Journal of Applied Polymer Science 2002;86(8):2079–84.
[12] Badaire S, Poulin P, Maugey M, Zakri C. Langmuir 2004;20(24):10367–70.
[13] Branca C, Magazu V, Mangione A. Diamond and Related Materials 2005; 14(3–7):846.
[14] Folkes MJ. Short fibre reinforced thermoplastics. 1st ed. Chichester, New York, Brisbane, Toronto, Singapore: Research Studies Press, Division of John Wiley & Sons; 1985.
[15] Pyrograf Products Incorporated: Pyrograf III, In: http://www.apsci.com/ppi-pyro3.html.
[16] Hine PJ, Tsui S-W, Coates PD, Ward IM, Duckett RA. Composites – Part A: Applied Science and Manufacturing 1997;28(11):949–58.
[17] Fan Z, Hsiao K-T, Advani SG. Carbon 2004;42(4):871–6.
[18] Ma H, Zeng J, Realff ML, Kumar S, Schiraldi DA. Composites Science and Technology 2003;63(11):1617–28.
[19] Wei C, Xiaoming T, Pu X, Xiaoyin C. Applied Surface Science 2005;252(5):1404.
[20] Lertwimolnun W, Vergnes B. Polymer 2005;46(10):3462–71.
[21] Foster RJ. The incorporation of carbon nanofibres to enhance the properties of hot compacted self-reinforced single polymer composites, in School of Physics and Astronomy. Leeds: University of Leeds; 2008.
[22] Patton RD, Pittman Jr CU, Wang L, Hill JR. Composites – Part A: Applied Science and Manufacturing 1999;30(9):1081.
[23] Brandl W, Marginean G, Chirila V, Warschewski W. Carbon 2004;42(1):5.
[24] Cox HL. British Journal of Applied Physics 1952;3:72–9.
[25] Krenchel, H. Akademisk Forlag; 1964.
[26] Tibbetts GG, Beetz Jr CP. Journal of Physics D (Applied Physics) Carbon Fibres – Properties and Applications 15–17 Sept. 1986;20(3):292–7.
[27] Hull D, Clyne TW. An introduction to composite materials. 2nd ed. Cambridge, New York, Melbourne: Cambridge University Press; 1996.